Nanoscale

PAPER

View Article Online
View Journal | View Issue

Cite this: *Nanoscale*, 2014, **6**, 1153

A DFT study of oxygen dissociation on platinum based nanoparticles†

Paul C. Jennings,[a] Hristiyan A. Aleksandrov,[bc] Konstantin M. Neyman[bd] and Roy L. Johnston*[e]

Received 5th September 2013
Accepted 13th November 2013

DOI: 10.1039/c3nr04750d

www.rsc.org/nanoscale

Density functional theory calculations are performed on 38 and 79 metal atom truncated octahedron clusters to study oxygen dissociation as a model for the initial stage of the oxygen reduction reaction. Pure platinum and alloyed platinum–titanium core–shell systems are investigated. It is found that barrierless oxygen dissociation occurs on the (111) facet of the pure platinum clusters. A barrier of ~0.3 eV is observed on the (100) facet. For the alloyed cluster, dissociation barriers are found on both facets, typically ~0.6 eV. The differences between the two systems are attributed to the ability of oxygen to distort the (111) surface of the pure platinum clusters. We show that flexibility of the platinum shell is crucial in promotion of fast oxygen dissociation. However, the titanium core stabilises the platinum shell upon alloying, resulting in a less easily distortable surface. Therefore, whilst an alloyed platinum-titanium electrocatalyst has certain advantages over the pure platinum electrocatalyst, we suggest alloying with a more weakly interacting metal will be beneficial for facilitating oxygen dissociation.

1 Introduction

The behaviour of oxygen (O) on platinum (Pt) surfaces has been studied extensively,[1–8] although much of the current work is focused on bulk systems, some studies have been performed on smaller cluster systems.[9–12] The interest in Pt–O systems is due in part to the relevance of Pt based catalysts in many industrial applications. A good example, is the extensive use of Pt to catalyse the oxygen reduction reaction (ORR) in fuel cells.[13–16] However, to develop and successfully market polymer electrolyte fuel cells (PEFCs), it is necessary to reduce the Pt catalyst loading of both anode and cathode electrodes, together with the associated cost, without compromising the performance.

The high intrinsic cost of Pt (£843.23 per ounce as of 10/07/13) forms a barrier to the widespread commercialisation of PEFCs. A ten-fold decrease in Pt loading in PEFC stacks is required to make PEFCs a commercially viable option. There are several ways to do this: lower the Pt loading by using a Pt alloy (either binary or ternary);[17,18] replace Pt with a non-precious electrocatalyst (inorganic or organic);[19,20] maximise the effective surface area of the Pt catalyst *i.e.* the surface contact between the electrode catalyst layers, the carbonaceous electronic conductor-gas diffusion layer, the polymer electrolyte membrane and the reactants (hydrogen and oxygen).[21,22]

Another serious problem with PEFCs is that the hydrogen feed usually contains significant amounts of carbon monoxide (CO), which poisons the Pt electrocatalyst. Alloying Pt to reduce loading and improve catalytic characteristics such as performance, durability and reactivity is a promising approach. We previously reported the results of theoretical calculations which suggested that alloying Pt with titanium (Ti), a much cheaper transition metal (£0.28 per ounce as of 10/07/13), to form Ti@Pt core–shell clusters (Ti – core, Pt – shell), results in weaker binding of hydroxyl (OH) and CO with reduced Pt loading.[23] Weaker binding of OH can lead to improvements in ORR kinetics, while weakening of CO binding lessens poisoning effects. Weaker adsorption was attributed to changes in the electronic structure attained through alloying; specifically, changes in the *d*-band centre.[24] At the same time the catalyst has to facilitate the initial stage of ORR, namely O_2 dissociation.

In our present work, oxygen dissociation is studied on pure Pt clusters as well as core–shell Ti@Pt clusters. Dissociation on the (111) slab model is also included, as this can represent the process on (111) terraces of larger particles. Initially focusing on 38 atom clusters, barrier-free dissociation is observed for the Pt_{38} cluster on the (111) facet. However, notable dissociation barriers are observed for the (100) facet as well as both (111) and (100) facets on the $Pt_{32}Ti_6$ cluster. This behaviour is explained through an in depth study of cluster stability and is further investigated for 79 atom clusters.

[a]*School of Chemical Engineering, University of Birmingham, Edgbaston, Birmingham, UK*
[b]*Departament de Química Física & IQTCUB, Universitat de Barcelona, Spain*
[c]*Faculty of Chemistry and Pharmacy, University of Sofia, Sofia, Bulgaria*
[d]*Institució Catalana de Recerca i Estudis Avançats (ICREA), Barcelona, Spain*
[e]*School of Chemistry, University of Birmingham, Edgbaston, Birmingham, UK. E-mail: r.l.johnston@bham.ac.uk; Fax: +44 (0)121 414 4403; Tel: +44 (0) 121 414 7477*

† Electronic supplementary information (ESI) available. See DOI: 10.1039/c3nr04750d

2 Methodology

Calculations are performed using the Vienna *Ab initio* Simulation Package (VASP) 5.2.[25–28] The $5d^9\ 6s^1$ of Pt, $3d^3\ 4s^1$ of Ti and $2s^2\ 2p^4$ of O are treated as valence electrons, while the ionic cores are represented by the projected augmented wave (PAW) method.[29,30] Electronic exchange and correlation are described using the generalised gradient approximation (GGA) using the Perdew Wang 91 (PW91) functional.[31,32] The Methfessel-Paxton smearing method is used with a width of 0.1 eV (extrapolated for computing final energies to zero smearing) and an energy cutoff of 415 eV is employed. DFT-D calculations were also performed on a number of test cases, although the inclusion of van der Waals forces through the empirical treatment of Grimme results in little change and so was not considered in the following results.

The bulk systems were modelled by five layers of repeated 3×3 (111) slabs, allowing the top two layers of the Pt(111) slab to relax fully while fixing the bottom 3 layers. A $5 \times 5 \times 1$ k point mesh was used to sample the first Brillouin zone. Approximately 10 Å of vacuum was included between neighbouring systems. For the cluster systems, 38 and 79 atom clusters were considered, these are magic numbers leading to complete Truncated Octahedral (TO) structures. The clusters are placed in the centre of a large enough supercell to ensure sufficient separation (~10 Å) between periodic images, the Γ point is used to sample the Brillouin zone. All atoms are relaxed according to the calculated atomic forces, with convergence criteria for total energies 1.0×10^{-4} eV and forces required to be less than 0.02 eV $Å^{-1}$.

In order to assess the (atomic or molecular) oxygen adsorption strength to the Pt surface, the binding energy (E_b) is calculated, as defined in eqn (1).

$$E_b = E_{AB} - (E_A + E_B) \quad (1)$$

E_{AB} is the energy of the cluster with oxygen adsorbed, E_A is the energy of the relaxed cluster and E_B is the energy of the free oxygen atom or molecule, negative E_b values imply favourable binding. The interaction energy (E_{int}) is defined in eqn (2).

$$E_{int} = E_{AB} - (E_A^* + E_B^*) \quad (2)$$

The single point energies of species distorted upon adsorption are denoted by *, again negative values imply favourable interactions. Distortion energies can be calculated using eqn (3) for $Pt_{n-m}Ti_m$ (where $n = 38$, 79 and $m = 0$, 6, 19) and eqn (4) for oxygen distortions.

$$\Delta E(Pt_{n-m}Ti_m) = E(Pt_{n-m}Ti_m) - E(Pt_{n-m}Ti_m)^* \quad (3)$$

$$\Delta E(O_2) = E(O_2) - E(O_2)^* \quad (4)$$

Although specific distortions, brought about by adsorption of oxygen, are discussed in detail, as a more general measure root mean squared displacements (RMSD) of atoms are calculated. RMSD is calculated as defined in eqn (5).

$$RMSD = \sqrt{\left(\frac{1}{N}\sum_{i=1,N} M_i - M_i^*\right)^2} \quad (5)$$

N is the total number of atoms, M_i is the position of a given atom (between 1 and N) for the relaxed bare cluster and M_i^* is the position of the same atom in the cluster following oxygen adsorption. Prior to applying this equation, a rotation and translation operator is used to align each cluster, thereby minimising the RMSD.

Dissociation pathways were investigated using the VASP Transition State Tools (VTST) implementation by the Henkelman Group, first generating an approximate pathway using the Nudged Elastic Band (NEB) method,[33] with further refinements achieved using the Dimer method.[34] Bader charge analysis[35] was performed using the Bader code[36] also from the Henkelman Group.

3 Results and discussion

3.1 Slab model

Large metal nanoparticles are often approximated in computational studies of catalysts by infinite slab models of (111) surface.[37] Hence, we start our study investigating O_2 dissociation on slabs. There are four non-symmetry equivalent sites on the surface of the infinite (111) slab, the atop, bridge, *fcc* and *hcp* sites. It is found that the bridge and *fcc* sites are energetically competitive, the E_b for O_2 at the bridge site being −0.87 eV, while it is −0.86 eV for the *fcc* position. This is in good agreement with experimental and theoretical studies, which have found both sites favourable for O_2 chemisorption.[38–42] The *hcp* site is 0.1 eV higher in energy than the *fcc* site (at −0.76 eV), while migration occurs when locally minimising O_2 at the atop position, resulting in O_2 bonding to the more favourable *fcc* site.

For the Pt(111) system, the oxygen molecule is initially adsorbed on a three-fold *fcc* hollow site, before dissociating resulting in each O atom being bound to *fcc* hollow sites. The dissociation barrier on the Pt(111) slab is found to be 0.45 eV, in agreement with other calculations, which find a barrier of between 0.4 and 0.6 eV, presented in the literature[1,5,43–45] as well as experimental studies.[46] An O–O distance of 2.10 Å is found at the transition state (TS) structure, this compares to an O–O distance of 1.40 Å for the initial state (IS) and 1.24 Å in the gas phase O_2. Significant elongation of the O–O bond suggests a late transition state. The average Pt–Pt bond lengths in the *fcc* sites below the adsorbate for the IS, TS and final state (FS) structures are close 2.94, 2.98 and 2.97 Å, respectively. However, the average Pt–Pt bond lengths for the pure Pt(111) surface is found to be 2.82 Å for the *fcc* hollow. This shows slight elongation of the Pt–Pt bond length when O_2 is adsorbed, by ≤0.15 Å. This is reflected in the relatively low RMSD values of 0.03, 0.05 and 0.05 Å, respectively, for IS, TS and FS structures. It is expected that a shortening of the Pt–O bond will be observed, corresponding to increased interactions with the Pt surface as O_2 dissociates. Indeed, average Pt–O bond lengths are 2.14, 1.95 and 2.05 Å for the IS, TS and FS, respectively.

The distortion energy of the bulk slab ($\Delta E(Pt_{surf})$) is found to be 0.17, 0.25 and 0.39 eV for the IS, TS and FS, respectively. Greater distortion of the surface is generally expected as the system progresses from the IS to the FS due to greater Pt–O interactions and a reduction in O–O interactions. $\Delta E(O_2)$ values calculated for the IS, TS and FS are 0.64, 5.72 and 6.34 eV, respectively. The average charge on the Pt atoms directly below O_2 is +0.18, +0.34

and +0.29 |e| for the IS, TS and FS. While overall average charges on O_2 are −0.34, −0.57 and −0.76 |e| for the IS, TS and FS, respectively. For all states, electron density is withdrawn from Pt by O, with increased charge transfer as the system progresses form the IS to the FS. There is greater Pt charge transfer when comparing the TS to the FS, this is due to O_2 being bonded to one 3-fold *fcc* hollow site at the TS and two at the FS.

We also considered PtTi (111) alloyed system, with a model (which has been studied before[47]) where the second layer of the slab was set as Ti and the top three layers (Pt–Ti–Pt) were allowed to fully relax. During the geometry optimization, however it shows instability and surface and subsurface layers can no longer be identified as (111). In order to study a more realistic model of the PtTi(111) alloyed system, we considered Ti@Pt nanoparticles, with Ti cores, where the effect of edges, larger flexibility, *etc.* can be taken into account. We studied two model clusters consisting of 38 and 79 metal atoms.

3.2 38 Atom clusters

3.2.1 Oxygen adsorption. On the surface of the 38 atom TO cluster there are eight symmetry inequivalent sites for a pure surface composition of the monometallic and alloyed core–shell clusters, shown in Fig. 1. Adsorption studies of atomic and molecular oxygen are performed on all non-symmetry equivalent sites. E_b values are then calculated, the results of which can be found in Table 1. Two possible bonding orientations are studied for O_2 adsorption, axial and planar. The axial configuration has O_2 bound to the surface through one O atom. The planar configuration is bound parallel to the surface, where the adsorbate position is defined in the following by the position of the middle of the O–O bond. It is found that the planar conformation is favourable in all cases, hence only those values are listed in Table 1.

For the pure Pt_{38} cluster, three-fold hollow positions 6 and 7 on the (111) facets, as well as the edge bridge position 5 between the (111) and (100) facets are the most stable for adsorption of atomic oxygen, −5.21, −5.12 and −5.12 eV, respectively. Interestingly, on $Pt_{32}Ti_6$, three-fold hollow positions are no longer locally stable and move to bridge sites (4 and 5). Position 5 is the most stable site, with an E_b value of −4.78 eV, a decrease of 0.34 eV with respect to the same position on the pure Pt_{38} cluster.

For O_2 adsorption, position 5, the edge-bridge site between (111) and (100) facets is most stable on both Pt_{38} and $Pt_{32}Ti_6$, E_b values are −2.01 and −1.75 eV, respectively. Hollow positions 6 and 7 are next in stability, −1.84 and −1.80 eV, on Pt_{38}, while on $Pt_{32}Ti_6$ other bridge positions are more favourable. Edge-bridge sites are also found to be positions of favourable O_2 bonding in other studies. Step sites on Pt(111) surfaces have been reported to result in particularly stable oxygen bonding.[48,49] Furthermore, studies of Pt TO clusters has revealed favourable bonding at the edge-bridge sites.[50] Calculations on the Pt(100) surface have favoured bonding to bridge sites, in line with the results presented here.[51] As with the previous OH and CO adsorption studies,[23,24] weaker bonding for O_2 and O is calculated for the bimetallic Ti@Pt cluster when compared with the pure Pt cluster.

Table 1 Calculated binding energies (E_b) for atomic and molecular oxygen on all non-symmetry equivalent sites of the 38 atom clusters, shown in Fig. 1. Values not presented are the result of oxygen migration to other sites during relaxation, as labeled. All energies are given in eV

Site	Position	Pt_{38}–O	Pt_{38}–O_2	$Pt_{32}Ti_6$–O	$Pt_{32}Ti_6$–O_2
1	Top	−4.17	−0.51	—[a]	—[b]
2	Top	−4.48	−0.77	−4.16	−0.59
3	bridge	—[b]	−1.66	—[a]	−0.57
4	bridge	−4.72	−1.67	−4.39	−1.02
5	bridge	−5.12	−2.01	−4.78	−1.75
6	*hcp*	−5.21	−1.84	—[c]	−0.73
7	*fcc*	−5.12	−1.80	—[a]	−0.37
8	4-fold hollow	−4.79	—[c]	−4.25	—[c]

[a] Adsorbate migration to position 4. [b] Adsorbate migration to position 6. [c] Adsorbate migration to position 5.

It is expected that oxygen dissociation will occur preferentially at sites with higher E_b values, where oxygen is most likely to adsorb to the surface of the cluster. Due to the small size of the cluster, it would be relatively easy for molecular oxygen to dissociate and migrate to any of the other seven sites, or an equivalent site in a different location on the surface. It is therefore assumed that dissociation will also likely result in atomic oxygen being adsorbed on the most energetically favourable sites. The energetic ordering of adsorption for molecular oxygen was similar to that of atomic oxygen, making the proposed dissociation pathways relatively straightforward.

The most stable sites, the edge site 5, as well as hollow sites 6 and 7 are studied. For each pathway, O_2 dissociation proceeds from one site to an adjacent position at an equivalent site (*e.g.* O_2 bound to position 5 dissociates to atomic oxygen bound to separate 5 sites). Data for each dissociation pathway is presented in Table 2. In each case, distortion energies of the cluster and O_2 at each step of the dissociation pathway are presented.

3.2.2 Distortion and interaction energies. Representations of the minimised geometries for the IS, TS and FS can be found in Fig. S5–S10.† Studies of the IS show that the distortion energy values ($\Delta E(Pt_{n-m}Ti_m)$) associated with Pt_{38} clusters are higher than those for the $Pt_{32}Ti_6$ clusters. The distortion energies associated with both clusters are also found to be greater than those for the pure slab, in most cases. O_2 distortion energies ($\Delta E(O_2)$) show greater distortions of the O_2 molecule adsorbed on Pt_{38} compared with $Pt_{32}Ti_6$ for the IS structures. However, as

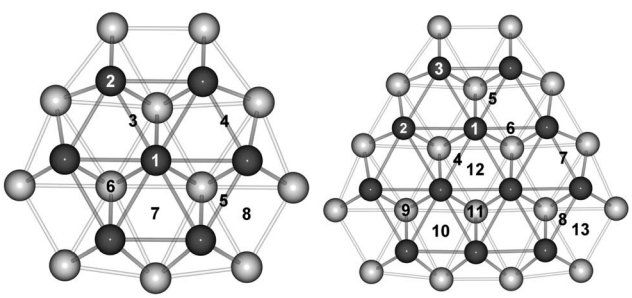

Fig. 1 Top view of the surface (dark grey) and subsurface (light grey) metal atoms at (111) facet sites on the 38 (left) and 79 (right) atom TO clusters.

Table 2 Values for cluster ($\Delta E(Pt_{n-m}Ti_m)$) *and oxygen* ($\Delta E(O_2)$) deformation energies, root mean squared displacements (RMSD) of the cluster, interaction energies (E_{int}), binding energies (E_b) and barriers for O_2 dissociation ($\Delta E^{\neq}$). The ratios of distortion energy to RMSD ($\Delta E(Pt_{n-m}Ti_m)$/RMSD) are also presented. Site numbering is introduced in Fig. 1. All energy values are given in eV, RMSD in Å

	$\Delta E(Pt_{n-m}Ti_m)$	RMSD	$\Delta E(Pt_{n-m}Ti_m)$/RMSD	$\Delta E(O_2)$	E_{int}	E_b	$\Delta E^{\neq}$
Initial state							
Pt_{38}-5	0.42	0.09	4.67	0.58	−3.02	−2.01	
$Pt_{32}Ti_6$-5	0.37	0.07	5.29	0.49	−2.62	−1.76	
Pt_{38}-6	0.45	0.19	2.37	1.05	−3.34	−1.84	
$Pt_{32}Ti_6$-6	0.12	0.03	4.00	0.73	−1.59	−0.74	
Pt_{38}-7	0.53	0.19	2.79	1.36	−3.68	−1.79	
$Pt_{32}Ti_6$-7	0.34	0.06	5.67	0.69	−1.40	−0.38	
Pt(111) Slab	0.17[a]	0.03	5.67[a]	0.64	−1.67	−0.86	
Transition state							
Pt_{38}-5	0.39	0.08	4.88	4.64	−6.72	−1.68	0.32
$Pt_{32}Ti_6$-5	0.62	0.10	6.20	4.89	−6.62	−1.11	0.62
Pt_{38}-6	0.48	0.19	2.53	2.75	−5.03	−1.80	0.04
$Pt_{32}Ti_6$-6	0.80	0.11	7.27	2.69	−3.90	−0.41	0.34
Pt_{38}-7	0.54	0.19	2.84	1.83	−4.16	−1.79	0.00
$Pt_{32}Ti_6$-7	0.44	0.07	6.29	5.29	−5.50	0.24	0.62
Pt(111) Slab	0.25[a]	0.05	5.00[a]	5.72	−6.41	−0.43	0.45
Final state							
Pt_{38}-5	0.58	0.10	5.80	6.27	−9.87	−3.02	
$Pt_{32}Ti_6$-5	0.35	0.06	5.83	6.36	−9.06	−2.36	
Pt_{38}-6	0.65	0.11	5.91	6.29	−10.32	−3.39	
$Pt_{32}Ti_6$-6	0.38	0.06	6.33	6.79	−10.13	−2.95	
Pt_{38}-7	0.92	0.22	4.18	6.28	−10.07	−2.87	
$Pt_{32}Ti_6$-7	0.86	0.10	8.60	6.79	−10.17	−2.51	
Pt(111) Slab	0.39[a]	0.05	7.80[a]	6.34	−9.12	−2.39	

[a] Values for $\Delta E(Pt_{surf})$.

mentioned previously, larger in magnitude adsorption energies are observed for the Pt_{38} clusters compared to the $Pt_{32}Ti_6$ clusters. This suggests that the increased interaction energy of O_2 to the Pt surface of the pure cluster, overcomes the distortion energies to a greater extent than for the bimetallic clusters. Furthermore, the stronger Pt–O binding will likely aid in distorting both oxygen and the Pt_{38} cluster to a greater degree than the $Pt_{32}Ti_6$ cluster. $\Delta E(O_2)$ values calculated for the bulk system are found to be greater than those on the (100) facet of both clusters, however smaller than on the (111) facet. The greater distortions on the cluster (111) facets compared to those on the slab are likely due to the increased binding energies on the clusters.

Distortion energies in the TS structures show, in general, that there is a greater distortion energy associated with the $Pt_{32}Ti_6$ clusters. The one exception is where distortion occurs on site 7 of the $Pt_{32}Ti_6$ cluster, due to different types of TS structures. In this case, a "straight" dissociation pathway is located over the central atop position (site 1) of the $Pt_{32}Ti_6$ cluster. For dissociation on site 6, however, a more curved pathway is preferred, avoiding the atop position and instead progressing over the hollow sites of the alloyed cluster. However, the fact that the distortion energies for the $Pt_{32}Ti_6$ clusters are significantly higher than for the Pt_{38} clusters suggests that the presence of the Ti core in the alloyed cluster stabilises (makes more rigid) the Pt shell. Nevertheless, the alloyed cluster is still distorted by the adsorbate. In all cases, the cluster distortion energies are greater than that of the slab, suggesting that the slab is significantly harder to distort than both clusters at the TS leading to little change in the slab structure. Similar to IS, data for the FS show the distortion energies associated with the Pt_{38} clusters are higher than those for the alloyed $Pt_{32}Ti_6$ clusters in all cases. Once again, there is generally greater distortion energies associated with the clusters than the slab. This was found to be the case also for positions 5 and 6.

For the pure Pt clusters, the IS and TS have similar distortion energies, the FS is found to have slightly greater distortion energies. This is consistent with atomic oxygen having a greater effect on the Pt surface than the single O_2 molecule. For the $Pt_{32}Ti_6$ clusters, it is found that the TS generally has greater distortion energies than the IS or FS. The exception to this is dissociation occurring at position 7, where a relatively small distortion energy is found at the TS compared to a relatively high energy at the FS. In summary, this energetic ordering suggests that at sites 5 and 6 greater distortions occur at the TS, not the FS as with the pure Pt clusters.

RMSD of the metal atoms are also listed in Table 2, it is important to note that O_2 distortions are not accounted for. These indicate the geometric distortion of the metal particle due to adsorption of the O_2 molecule. Data on distortions to specific facets of the cluster are described later. For RMSD analysis, the geometry of the distorted cluster, with O_2 removed, is compared to the geometry of the relaxed gas phase cluster, with higher values suggesting greater distortion. For the Pt_{38} clusters, there is a larger RMSD associated with O_2 adsorption

on the (111) facet, compared to the (100) facet, an average of 0.19 and 0.09 Å, respectively. For the $Pt_{32}Ti_6$ clusters, there is less difference between O_2 adsorption on the (111) and (100) facets, 0.03–0.11 Å *vs.* 0.06–0.10 Å. Furthermore, it is found that smaller RMSD values for the bimetallic clusters can lead to greater distortion energies compared to the pure Pt clusters. This shows that even though there is less overall distortion, there is a greater energetic cost associated with it for the $Pt_{32}Ti_6$ clusters. This is expected, as the Pt_2 dimer binding energy is found to be −4.11 eV, which is destabilised over both the PtTi and Ti_2 = dimers, −6.08 and −5.34 eV, respectively. Comparing to the values calculated for the bulk system (RMSD < 0.05), there are significantly greater RMSD values associated with the Pt_{38} clusters and marginally greater values for the $Pt_{32}Ti_6$ cluster.

$\Delta E(Pt_{n-m}Ti_m)$/RMSD has been calculated, showing the energy needed to achieve RMSD of 1.00 Å. An average of 1.71, 3.17 and 1.63 eV $Å^{-1}$ more energy is required to distort the $Pt_{32}Ti_6$ cluster, than the Pt_{38} cluster at the IS, TS and FS, respectively. This demonstrates the significant energy barriers that need to be overcome in order to distort the $Pt_{32}Ti_6$ cluster compared to the Pt_{38} cluster.

A high dissociation barrier ($\Delta E^{\neq}$) is found for site 5, on the (100) facet of the $Pt_{32}Ti_6$ cluster, 0.62 eV, this being approximately twice that of the pure Pt_{38} cluster, 0.32 eV (Table 2). When considering the (111) facet of the $Pt_{32}Ti_6$ cluster, the dissociation barriers for sites 7 and 5 are equal, 0.62 eV, while for site 6 the barrier, 0.34 eV, is about half that of the other two sites. The Pt_{38} cluster is found to exhibit barrier-free dissociation on the (111) facet, this dramatically differs to the 0.45 eV barrier found on the Pt(111) slab. On the (100) facet of the Pt_{38} cluster (site 5), comparable dissociation barriers are found to site 6 on the $Pt_{32}Ti_6$ cluster.

3.2.3 Geometric analysis. Analysis of the system geometries can be found in Table 3. O–O bonds, in general, are shorter for the IS adsorption on the (100) facet. However, at the TS, generally shorter bond lengths are associated with the (111) facet. When studying the average Pt–O bond length, as the system moves from the IS to the TS, the average bond length gets smaller. The average Pt–Pt bond lengths are found to be 2.65, 2.70 and 2.70 Å for bond types 1 to 3, respectively (Fig. 2) for the bare Pt_{38} cluster, while for the bare $Pt_{32}Ti_6$ cluster, the corresponding Pt–Pt bond lengths are slightly larger, 2.69, 2.71 and 2.74 Å for sites 1 to 3, respectively.

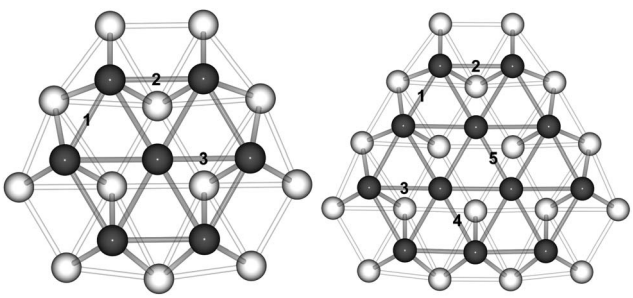

Fig. 2 Bond numbering on the 38 (left) and 79 atom (right) TO clusters.

Once oxygen is adsorbed on the (100) facet of the Pt_{38} cluster, significant elongation of bond type 2 by up to 0.54 Å is observed, although there is less overall distortion of the cluster geometry. Following oxygen adsorption on the (100) facet, the average distortion of the Pt–Pt bonds calculated from the data in Table 3 is 0.43, 0.53 and 0.78 Å for sites 5, 6 and 7 on the Pt_{38} cluster, respectively. When O_2 is adsorbed on the (111) facet, there is a slight elongation of bond type 1 by up to 0.29 Å, although not as much as for bond type 3 by up to 0.85 Å, which is significantly elongated. There is generally a slight contraction in the bond length of type 2 by up to 0.06 Å. This suggests that the majority of the distortion that occurs when O_2 is adsorbed on the (111) facet of the Pt_{38} cluster is due to changes in the bond length of type 3, bonding to the central (111) atom. For the $Pt_{32}Ti_6$ cluster significant elongation is observed of bond type 2 by up to 0.57 Å, when O_2 is adsorbed on site 5 of the (100) facet. However, there is considerably less distortion of the other bond types when O_2 is adsorbed on the (111) facet, the maximum distortion observed being ≤0.37 Å.

Pt–X^{centre} values are only calculated for dissociations on the (111) facet. From the values presented in Table 4, there are few well-defined trends when comparing initial, transition and final states. However, the point of these values is to demonstrate the differences between the Pt_{38} and $Pt_{32}Ti_6$ clusters. Pt–X^{centre} was calculated by defining a plane through the cluster, parallel to the (111) facet on which oxygen is adsorbed and then measuring Pt distortions along the *y*-axis from that plane. The plane passes through the central atoms of the (111) surfaces surrounding the facet on which the O_2 is adsorbed, as shown in Fig. 3.

Following O_2 adsorption, Pt–X^{centre} distances are presented in Table 4. This reveals small distortions, ≤ 0.14 and ≤ 0.08 Å for the Pt_{38} and $Pt_{32}Ti_6$ clusters, respectively, measuring distances from the plane to the bottom of the cluster. More significant changes are seen at the top of the cluster, ≤0.91 and ≤0.42 Å for the Pt_{38} an $Pt_{32}Ti_6$ clusters, respectively. Furthermore, it is found that there is considerably stronger distortion of the Pt_{38} cluster, with the atop central (111) atom being pulled out of the plane. The relationship between Pt–X^{centre} and distortion barriers can be seen in Fig. S1 and S2† for the IS and TS.

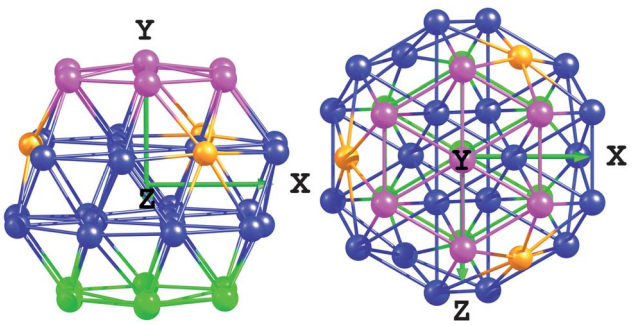

Fig. 3 Splitting the cluster into top and bottom portions to analyse relevant movement of the plane defined to measure distortions. Pink atoms are at the top of the cluster, whilst green are at the bottom. The plane passes through the centre of the adjoining (111) surfaces to that at which the O_2 is adsorbed, in this case depicted by the orange atoms.

Table 3 Data for oxygen–oxygen distances (O–O), average platinum–oxygen bond lengths (Pt–O), average platinum–platinum bond lengths (Pt–Pt) for specific bonds defined in Fig. 2 and distances from the octahedral core to the central (111) atom in the *y*-direction (Pt–X^{centre}). Average Pt–Pt bond lengths are calculated for those atoms directly below the adsorbed O_2 molecule. The type of the bond is shown in brackets according to Fig. 2. All values are given in Å

	O–O			Pt–O			Pt–Pt			Pt-X^{centre}		
	IS	TS	FS	IS	TS	FS	IS	TS	FS	IS	TS	FS
Pt_{38}-5	1.39	1.92	2.89	1.95	1.82	1.95	$3.24^{[2]}$	$3.20^{[2]}$	$2.94^{[2]}$	—	—	—
$Pt_{32}Ti_6$-5	1.37	1.96	3.02	1.98	1.83	1.98	$3.26^{[2]}$	$3.28^{[2]}$	$2.93^{[2]}$	—	—	—
Pt_{38}-6	1.45	1.66	3.32	2.07	2.00	2.07	$2.64^{[2]}$ $3.43^{[3]}$	$2.65^{[2]}$ $3.44^{[3]}$	$2.69^{[2]}$ $2.93^{[3]}$	3.27	3.26	2.95
$Pt_{32}Ti_6$-6	1.41	1.66	5.43	2.21	2.13	1.98	$2.92^{[2]}$ $2.74^{[3]}$	$3.02^{[2]}$ $3.04^{[3]}$	$2.94^{[2]}$	2.19	2.72	2.08
Pt_{38}-7	1.49	1.55	3.42	2.05	2.02	1.94	$2.68^{[1]}$ $3.54^{[3]}$	$2.69^{[1]}$ $3.55^{[3]}$	$2.95^{[1]}$ $2.98^{[3]}$	3.27	3.26	3.35
$Pt_{32}Ti_6$-7	1.40	2.03	5.47	2.19	1.99	1.95	$2.78^{[1]}$ $2.78^{[3]}$	$2.93^{[1]}$ $2.79^{[3]}$	$3.06^{[1]}$	2.12	2.23	2.11

Table 4 Pt–X^{centre} distances relative to those of the bare clusters. Positive values show atoms being drawn out of the plane, leading to elongation of the cluster in the *y*-direction, whilst negative values show compression of the cluster in the *y*-direction. All values are given in Å

	IS		TS		FS	
	Top	Bottom	Top	Bottom	Top	Bottom
Pt_{38}-6	0.83	0.13	0.82	0.14	0.51	0.14
$Pt_{32}Ti_6$-6	−0.12	0.07	0.42	0.04	−0.23	0.08
Pt_{38}-7	0.83	0.00	0.82	0.00	0.91	0.00
$Pt_{32}Ti_6$-7	−0.18	0.03	−0.07	0.04	−0.19	0.02

Table 5 Average charges (|e|) of the initial (IS), transition (TS) and final (FS) state structures of O_2 dissociation on the 38 atom clusters

	Pt charges[a]			Ti charges[b]			O charges		
	IS	TS	FS	IS	TS	FS	IS	TS	FS
Pt_{38}-5	0.31	0.46	0.45	—	—	—	−0.33	−0.51	−0.74
$Pt_{32}Ti_6$-5	0.04	0.22	0.21	1.97	1.97	1.88	−0.34	−0.55	−0.75
Pt_{38}-6	0.22	0.29	0.28	—	—	—	−0.39	−0.47	−0.76
$Pt_{32}Ti_6$-6	−0.22	0.02	0.11	1.95	1.87	1.94	−0.38	−0.50	−0.79
Pt_{38}-7	0.25	0.26	0.33	—	—	—	−0.43	−0.45	−0.74
$Pt_{32}Ti_6$-7	−0.23	−0.10	0.09	1.95	1.93	1.94	−0.37	−0.58	−0.76

[a] Pt atoms interacting directly with O atoms. [b] Ti atoms interacting directly with O bound Pt atoms.

3.2.4 Bader charge analysis. We previously studied charge transfer between Pt and Ti atoms within core–shell systems.[24] For reference, the electronegativities of Pt, Ti and O are 2.28, 1.54 and 3.44 on the Pauling scale, respectively. For the bare clusters, there is significant electron donation from Ti to Pt, which likely results in the strong core–shell interactions that stabilise the Pt surface. The average charges for the $Pt_{32}Ti_6$ cluster are found to be −0.36 and +1.94 |e| for Pt and Ti, respectively. Following this, an analysis was performed of the effect of the adsorbate on the atomic charges, as shown in Table 5.

When O_2 is adsorbed on the surface of the pure Pt_{38} cluster, the Pt atoms on which the oxygen is adsorbed have a positive charge +0.22 to +0.31 |e|. It is generally found on Pt_{38} and $Pt_{32}Ti_6$ clusters, that the Pt becomes more positively charged as the system moves from the initial to final states, while the O atoms become more negatively charged at the same time. Furthermore, more positive Pt charge values are observed for O_2 adsorption on the (100) facet. This charge transfer is found to be comparable between the slab and cluster models. In the case of the $Pt_{32}Ti_6$ cluster Pt has positive and negative charges depending on the state of the system, slightly positive (+0.04 |e|) when O_2 is adsorbed on the (100) facet and negative on the (111) facet (−0.22 to −0.23 |e|). At the same time, charges on the Ti atoms, which are remote from the adsorbates, do not change notably. They also do not change when the system progresses from IS to FS. Not surprisingly, the charges on the oxygen atoms get significantly more negative as the system progresses from the initial to the final states. This charge seems unaffected by the site at which oxygen is adsorbed, or whether it is the pure or alloyed cluster. Hence, one can conclude that O atoms have local effects on the withdrawal of electron density from the closest Pt atoms only. When O_2 is adsorbed on the (111) facet of the alloyed $Pt_{32}Ti_6$ nanoparticle, Pt is found to have a negative charge at the initial state and a positive charge at the final state, while on the (100) facet, the Pt atoms are positive for all states.

3.2.5 Conclusions. There are several conclusions that can be drawn from the 38 atom system. It is possible to see that there are significant differences in the Pt_{38} and $Pt_{32}Ti_6$ systems, not only in adsorption energies but also in the way dissociation proceeds. Larger dissociation barriers are observed for the $Pt_{32}Ti_6$ system. This is to be expected because oxygen is more weakly adsorbed onto the Pt surface of the alloyed cluster, hence the O–O bond is less activated and it therefore takes more energy to dissociate the O_2 molecule. Furthermore, for the Pt_{38} cluster, a higher dissociation barrier is observed for the (100) facet whereas for $Pt_{32}Ti_6$ there are similar barriers on the (111) and (100) facets. Once again, this coincides with the larger values of adsorption energies associated with the (111) facet for the Pt_{38} system and the (100) facet for the $Pt_{32}Ti_6$ system.

Finally, barrier-free dissociation is observed on the (111) facet of the Pt_{38} cluster which appears to be due to significant distortions of the facet. There are greater energetic costs associated with distorting the $Pt_{32}Ti_6$ cluster, compared with Pt_{38} cluster (Table 2). Although according to the cluster geometries there is greater distortion of the Pt_{38} cluster. This suggests that the presence of the octahedral Ti core in the $Pt_{32}Ti_6$ cluster stabilises the Pt shell and makes the structure more rigid, while Pt_{38} nanoparticle is more flexible and the surface Pt atoms become more easily distorted, hence more reactive. When compared to the Pt(111) bulk system, the barrier for O_2 dissociation is found to be 0.45 eV, however very little distortion of the (111) surface is observed. This supports the suggestion that it is the distortion of the (111) facet on the cluster that leads to barrier-free dissociation.

3.3 79 Atom clusters

3.3.1 Oxygen adsorption. Following the calculations on 38 atom clusters, studies progressed to larger 79 atom TO clusters, considering the pure Pt_{79} and core–shell $Pt_{60}Ti_{19}$ systems. On the surface of the 79 atom TO cluster there are 13 non-symmetry equivalent sites for a pure surface composition, depicted in Fig. 1. As with the 38 atom clusters, studies of these 13 sites are performed, looking at atomic and molecular oxygen. Binding energies are listed in Table 6.

For the pure Pt_{79} cluster, the hollow site on the (111) facet is no longer as favourable as the edge-bridge sites on the (100) facet for O_2 and O adsorption. However, the site resulting in strongest bonding is the edge-bridge site of the (111) facet, labelled as site 7. For the $Pt_{60}Ti_{19}$ cluster, in all cases, the edge-bridge site on the (100) facet results in strongest bonding. This was also the case for $Pt_{32}Ti_6$.

In a similar fashion to the 38 atom system, O_2 dissociation has been investigated at various sites on the (111) and (100) facets of the 79 atom clusters (8, 9, 10 and 11 in Fig. 1). Due to the increased size of the (111) facet, it is no longer beneficial to allow dissociation pathways from a certain site to an identical adjacent site, as this would span the entire facet. Following dissociation, any further barriers observed would be due to migration of the oxygen atoms over the surface, which is not the aim of this study. Therefore, for the 79 atom clusters, the pathways on the (111) facet terminate at the central site 12. As with the 38 atom clusters, dissociation on the edge-bridge site of the (100) facet proceeds from position 8 to two adjacent 8 sites.

The central positions on the (111) facet were also investigated, the hollow site 12 for the Pt_{79} cluster and site 4 on $Pt_{60}Ti_{19}$. However, relatively small O_2 binding energies, particularly on the $Pt_{60}Ti_{19}$ cluster, are associated with these sites. Hence, finding TS for O_2 dissociation proved difficult on these sites. The terrace site is unlikely to be active for oxygen dissociation due to the weaker Pt–O interactions associated with this position. On the 79 atom clusters, the central three-fold hollow site is surrounded by more favourable edge hollow and bridge sites. This means that it is far more likely that O_2 dissociation will occur at the edge sites of the facet, where stronger Pt–O bonding is observed. Furthermore, low-coordinated edge sites are able to distort to a greater extent (see below) than the central three-fold hollow site, hence facilitating lower barriers to O_2 dissociation.

3.3.2 Distortion and interaction energies. Representations of the minimised geometries for the IS, TS and FS can be found in Fig. S11–S18.† Table 7 shows distortion energies, for the cluster and oxygen as well as interaction, binding energies and dissociation barriers. The IS studies reveal slightly greater energetic penalties (by an average of 0.11 eV) associated with distorting the Pt_{79} cluster compared to the $Pt_{60}Ti_{19}$ cluster. This same trend is observed for the FS, with greater distortion energies located for the Pt_{79} cluster. These trends were also found for the smaller 38 atom clusters. However, the trends for the TS structures differ from those for the 38 atom clusters. For the 79 atom clusters, sites 8 and 11 result in greater distortion energies associated with the alloyed $Pt_{60}Ti_{19}$, whilst for sites 9 and 10, greater distortion energies are associated with Pt_{79}.

As for Pt_{38}, there are greater distortion energies associated with the FS compared to the IS or TS. This once again suggests that the strongly interacting atomic oxygen has a greater ability to distort the Pt_{79} surface. For $Pt_{60}Ti_{19}$, there are greater distortion energies associated with the TS and FS compared to the IS. RMSD analysis demonstrates that for the Pt_{79} cluster, there is generally least structural distortion when O_2 is adsorbed on position 9 on the (111) facet. Although, there is little difference between positions 8 on the (100) facet and 9 on the (111) facet. There is significant distortion of Pt_{79} when oxygen is adsorbed on sites 10 and 11. As with the 38 atom clusters, there is greater distortion of the pure Pt clusters, compared to the alloyed ones. For $Pt_{60}Ti_{19}$, there is generally little difference between the RMSD for the cases when O_2 is adsorbed on (111) and (100) facets, suggesting again that Ti@Pt structures are more rigid due to the strong interaction between Ti core and Pt shell.

When comparing the (111) and (100) facets, it is found that the Pt_{79} cluster distortion energy associated with site 8 on the

Table 6 Calculated binding (E_b) energies for atomic and molecular oxygen on the various sites of the 79 atom clusters. Values which have not been presented are the result of oxygen migration to other sites during relaxation, as labeled. All energies are given in eV

Site	Position	Pt_{79}–O	Pt_{79}–O_2	$Pt_{60}Ti_{19}$–O	$Pt_{60}Ti_{19}$–O_2
1	Top	—[a]	—[b]	−2.69	—[a]
2	Top	—[c]	−0.41	—[c]	−0.41
3	Top	−4.36	−0.71	−4.24	—[d]
4	Bridge	—[e]	−1.07	—[f]	−0.09
5	Bridge	—[g]	−1.45	—[c]	−0.77
6	Bridge	—[g]	−1.21	—[c]	−0.68
7	Bridge	−5.04	−1.83	−4.60	−1.15
8	Bridge	−4.94	−1.81	−4.93	−1.85
9	*hcp*	−4.93	−1.13	—[d]	−0.71
10	*fcc*	−4.98	−1.39	—[c]	−0.69
11	*hcp*	−4.74	−0.99	−3.79	−0.63
12	*fcc*	−4.93	−0.88	−3.32	0.07
13	4-fold Hollow	−4.83	—[d]	−4.56	—[d]

[a] Adsorbate migration to position 9. [b] Adsorbate migration to position 5. [c] Adsorbate migration to position 7. [d] Adsorbate migration to position 8. [e] Adsorbate migration to position 12. [f] Adsorbate migration to position 11. [g] Adsorbate migration to position 10.

Table 7 Cluster ($\Delta E(Pt_{n-m}Ti_m)$) and oxygen ($\Delta E(O_2)$) deformation energies, root mean squared displacements (RMSD) of the cluster, interaction energies (E_{int}), binding energies (E_b) of O_2 and barrier of O_2 dissociation ($\Delta E^{\neq}$). The ratios of distortion energy to RMSD ($\Delta E(Pt_{n-m}Ti_m)$/RMSD) are also presented. All energy values are given in eV, RMSD in Å

	$\Delta E(Pt_{n-m}Ti_m)$	RMSD	$\Delta E(Pt_{n-m}Ti_m)$/RMSD	$\Delta E(O_2)$	E_{int}	E_b	$\Delta E^{\neq}$
Initial state							
Pt_{79}-8	0.31	0.08	3.88	0.58	−2.69	−1.80	
$Pt_{60}Ti_{19}$-8	0.27	0.05	5.40	0.49	−2.60	−1.84	
Pt_{79}-9	0.13	0.06	2.17	0.80	−2.05	−1.12	
$Pt_{60}Ti_{19}$-9	0.12	0.02	6.00	0.71	−1.51	−0.68	
Pt_{79}-10	0.37	0.10	7.10	0.95	−2.71	−1.40	
$Pt_{60}Ti_{19}$-10	0.32	0.05	6.40	0.65	−1.64	−0.67	
Pt_{79}-11	0.50	0.13	3.85	0.88	−2.37	−0.99	
$Pt_{60}Ti_{19}$-11	0.17	0.03	5.67	0.47	−1.23	−0.59	
Pt(111) Slab	0.17[a]	0.03	5.67[a]	0.64	−1.67	−0.86	
Transition state							
Pt_{79}-8	0.22	0.10	2.20	0.78	−2.46	−1.46	0.34
$Pt_{60}Ti_{19}$-8	0.33	0.05	6.60	5.31	−6.81	−1.18	0.66
Pt_{79}-9	0.22	0.08	2.75	3.69	−4.81	−0.91	0.21
$Pt_{60}Ti_{19}$-9	0.15	0.03	5.00	5.02	−5.25	−0.08	0.60
Pt_{79}-10	0.73	0.18	4.06	2.23	−4.45	−1.49	0.00
$Pt_{60}Ti_{19}$-10	0.45	0.06	7.50	5.41	−5.86	0.00	0.69
Pt_{79}-11	0.45	0.15	3.00	1.14	−2.54	−0.95	0.05
$Pt_{60}Ti_{19}$-11	0.91	0.10	9.10	3.08	−3.82	0.17	0.77
Pt(111) Slab	0.25[a]	0.05	5.00[a]	5.72	−6.41	−0.43	0.45
Final state							
Pt_{79}-8	0.43	0.09	4.78	6.33	−9.50	−2.74	
$Pt_{60}Ti_{19}$-8	0.33	0.05	6.60	6.28	−8.91	−2.30	
Pt_{79}-9	1.38	0.16	8.63	6.28	−10.57	−2.91	
$Pt_{60}Ti_{19}$-9	0.40	0.05	8.00	6.79	−8.69	−1.50	
Pt_{79}-10	1.21	0.14	8.64	6.30	−10.47	−2.96	
$Pt_{60}Ti_{19}$-10	0.52	0.05	10.40	6.28	−7.92	−1.13	
Pt_{79}-11	1.41	0.16	8.81	5.94	−9.68	−2.33	
$Pt_{60}Ti_{19}$-11	0.42	0.05	8.40	6.79	−8.87	−1.66	
Pt(111) Slab	0.39[a]	0.05	7.80[a]	6.34	−9.12	−2.39	

[a] Values for $\Delta E(Pt_{surf})$.

(100) facet is greater than that for site 9 on the (111) facet of the Pt_{79} IS structure (Table 7). However, the distortion energies become equal at the TS but are 0.95 eV greater on site 9 for the FS structure. For sites 10 and 11 on the (111) facet, the distortion energy is greater than for site 8 in all cases. The $\Delta E(Pt_{79})$ values for sites 9, 10 and 11 correlate with the differences between the dissociation barriers between sites. The smallest $\Delta E(Pt_{79})$ value is for site 9 which also has the largest barrier, whilst site 10 has the largest $\Delta E(Pt_{79})$ value and smallest barrier. There is less correlation between cluster distortion energies, surface sites and dissociation barriers for the $Pt_{60}Ti_{19}$ system.

$\Delta E(Pt_{n-m}Ti_m)$/RMSD has also been calculated for the 79 atom clusters. An average of 1.62, 4.05 and 0.64 eV $Å^{-1}$ more energy is required to distort the $Pt_{60}Ti_{19}$ cluster, than the Pt_{79} cluster at the IS, TS and FS, respectively. This further demonstrates the significant energy barriers that need to be overcome in order to distort the $Pt_{60}Ti_{19}$ cluster compared to the Pt_{79} cluster.

Oxygen distortion values for the IS are greater for the Pt_{79} system, compared to the $Pt_{60}Ti_{19}$ system, in all cases. However, at the TS, significantly greater distortion energies are associated with the $Pt_{60}Ti_{19}$ clusters. This suggests that, initially, when oxygen is adsorbed on the surface of the Pt_{79} cluster, due to the stronger Pt–O interactions, the O_2 molecule is distorted to a greater extent than on the alloyed system, where weaker bonding is observed. However, at the TS, on the more weakly bound $Pt_{60}Ti_{19}$ system, greater distortion of the O_2 molecule is required, compared to the Pt_{79} system. This greater distortion requires more energy and can rationalise larger dissociation barriers on Ti@Pt compared to the pure Pt nanoparticle. The same discussion is also valid for Pt_{38} and $Pt_{32}Ti_6$ nanoparticles. O_2 distortion energies correlate with the corresponding O–O distances. Furthermore, the smaller difference in the O–O distances between the IS and TS for the Pt_{79} clusters compared to $Pt_{60}Ti_{19}$ clusters show that TS are "earlier" on Pt_{79}. Earlier TS are known to have lower barriers, which is found to be the case in this study.

Very similar dissociation barrier on the (100) facet are located for the 79 and 38 atom clusters (Tables 2 and 7). The dissociation barriers are about twice that for the alloyed clusters (0.62 and 0.66 eV for the $Pt_{32}Ti_6$ and $Pt_{60}Ti_{19}$ clusters, respectively) compared to the pure clusters (0.32 and 0.34 eV for the Pt_{38} and Pt_{79} clusters, respectively). However, for the dissociation barriers located on the (111) facet the relationship becomes a little more complicated.

Table 8 Data for oxygen–oxygen distances (O–O), average platinum–oxygen bond lengths (Pt–O), average platinum–platinum bond lengths (Pt–Pt) for specific bonds defined in Fig. 2 and distances from the octahedral core to the central (111) atom in the *y*-direction (Pt–X^{centre}). Average Pt–Pt bond lengths are calculated for those atoms directly below the adsorbed O_2 molecule. The type of the bond is shown in brackets according to Fig. 2

	O–O			Pt–O			Pt–Pt			Pt–X^{centre}		
	IS	TS	FS	IS	TS	FS	IS	TS	FS	IS	TS	FS
Pt_{79}-8	1.39	1.42	2.98	1.96	2.01	1.95	3.18[2]	3.03[2]	2.96[2]	—	—	—
$Pt_{60}Ti_{19}$-8	1.37	2.03	3.87	1.98	1.84	1.92	3.27[2]	3.22[2]	3.04[2]	—	—	—
Pt_{79}-9	1.42	1.79	3.94	2.14	2.00	2.02	2.77[2] 2.80[3]	2.83[2] 2.84[3]	2.78[2] 2.93[3] 3.11[5]	3.21	3.30	4.22
$Pt_{60}Ti_{19}$-9	1.41	1.98	5.03	2.22	2.02	2.10	2.91[2] 2.76[3]	2.89[2] 2.76[3]	2.97[2] 2.77[5]	2.96	3.00	2.95
Pt_{79}-10	1.44	1.60	3.17	2.08	2.00	2.04	2.72[1] 3.54[3] 3.53[4]	2.72[1] 3.54[3] 3.54[4]	2.74[1] 3.12[3] 3.19[4] 2.98[5]	4.01	4.01	3.93
$Pt_{60}Ti_{19}$-10	1.40	2.05	3.75	2.18	1.99	2.02	2.69[1] 2.85[3] 2.90[4]	2.72[1] 2.77[3] 2.91[4]	2.70[1] 2.75[5]	2.92	2.96	2.91
Pt_{79}-11	1.43	1.47	2.53	2.09	2.09	2.07	3.24[4] 2.73[5]	3.30[4] 2.76[5]	3.08[4] 3.11[5]	3.41	3.39	3.90
$Pt_{60}Ti_{19}$-11	1.37	1.71	4.89	2.33	2.13	2.09	2.90[4] 2.68[5]	2.71[1] 2.71[3] 3.09[4] 2.76[5]	2.71[1] 2.85[4]	2.94	3.11	2.91

For the Pt_{38} cluster, barrier-free dissociation was observed on sites 6 and 7 on the (111) facet. For the Pt_{79} cluster, once again almost barrier-free dissociation is located on sites 10 and 11. However, a dissociation barrier of 0.21 eV is found for dissociation on site 9. When comparing binding energies at sites 9 and 11, there is a small difference of 0.12 eV. Probably this difference is not simply a matter of different Pt–O bonding strengths but is related more to differences in the sites. Sites 9 and 11 are *hcp* whilst site 10 is *fcc*. This suggests that the difference in dissociation barriers is probably due to the neighbouring surfaces to which the sites are adjacent. Whilst site 9 is neighbouring a (100) facet, sites 10 and 11 both neighbour (111) facets, implying that the adjacent (100) facet distorts less than an adjacent (111) facet and results in the small dissociation barrier for site 9 on the Pt_{79} cluster (see Pt–X^{centre} values in Table 8). Finally, dissociation barriers on the (111) facet of the $Pt_{60}Ti_{19}$ clusters are similar to that of the (100) facet. Here again, correlation between barriers and Pt–X^{centre} values is found since Pt–X^{centre} values are also similar at both types of facets.

3.3.3 Geometric analysis. Again, it appears that the more easily distorted shell on the Pt_{79} cluster results in the observed barrier-free dissociation. Similar measurements to those performed for the 38 atom clusters, to quantify differences in distortions, are compiled in Table 8. Roughly comparable O–O bond lengths are observed for all initial states on the 79 atom clusters, 1.39–1.44 Å for the pure Pt_{79} nanoparticle and 1.37–1.41 Å for $Pt_{60}Ti_{19}$. At the TS, there are significantly shorter O–O bond lengths associated with the Pt_{79} cluster compared to those for the $Pt_{60}Ti_{19}$ clusters, 1.42–1.79 Å *vs.* 1.71–2.05 Å. Studying Pt–O bond lengths reveals a similar trend to those for the 38 atom clusters, where in general, shorter bond lengths are observed as the system progresses from the initial to the transition state.

The Pt–Pt bond lengths for the bare Pt_{79} cluster are 2.66, 2.73, 2.70, 2.75, 2.68 Å for bond types 1 to 5, respectively (Fig. 2). For site 8 on the (100) facet, significant distortion (by an average of 0.33 Å) of bond type 2 is observed. However, for the initial and transition states this is unsurprising as O_2 is interacting with the one bond. Therefore, although there is significant elongation of bond type 2, there is less overall distortion of the cluster. Bond types 3 and 4 are distorted (by an average of 0.42 and 0.56 Å, respectively) to the greatest extent for O_2 adsorption on the (111) facet. The elongation of bonds surrounding the hollow sites at which oxygen is adsorbed on the (111) facet leads to greater overall distortions of the cluster.

The Pt–Pt bond lengths of the alloyed $Pt_{60}Ti_{19}$ cluster are 2.68, 2.84, 2.73, 2.75 and 2.73 Å for bond types 1 to 5, respectively. Once again, significant elongation of bond type 2 is observed on the (100) facet when O_2 is adsorbed, 0.34 Å, although as with the Pt_{79} cluster, little overall distortion of the cluster is observed, $\leq$0.10 Å. There is far less distortion of other bond types when studying dissociation on the (111) facet. This is expected as there appears to be far less distortion of the overall cluster geometries upon adsorbing O_2.

Pt–X^{centre} values for the bare pure Pt_{79} cluster are 3.15 and 6.29 Å for the top and bottom of the cluster, respectively. For the bare $Pt_{60}Ti_{19}$ cluster, these values are found to be 3.02 and 6.05 Å. Once again, there is considerable distortion of the Pt_{79} cluster when O_2 is adsorbed on the (111) facet, with Pt–X^{centre} distances elongated by up to 1.07 Å (Table 9). There is less distortion of the IS (111) facet (Pt–X^{centre} – 0.06 Å) associated with site 9, where a small dissociation barrier of 0.21 eV is observed. Less

distortion is also observed for the $Pt_{60}Ti_{19}$ clusters, with generally even a slight contraction in the Pt–X^{centre} values. More detailed analysis of the changes in Pt–X^{centre} can be found in Table 9, once again showing little deviation in distances from the plane to the bottom of the cluster. The relationship between Pt–X^{centre} and dissociation barriers can be seen in Fig. S1 and S2† for the IS and TS, again allowing for further comparisons between the 38 and 79 atom clusters.

3.3.4 Bader charge analysis. Charge analysis is performed, the results of which are given in Table 10. The charges for the bare $Pt_{60}Ti_{19}$ cluster are −0.45 and +1.43 for Pt and Ti atoms, respectively. For the pure Pt_{79} cluster, similar to the Pt_{38} case, a positive charge is found on the Pt atoms interacting with the oxygen. These charges generally get more positive as the system progresses from the initial to final state. Again, this coincides with the charge on the oxygen becoming more negative.

For the $Pt_{60}Ti_{19}$ clusters, the charges on the Pt atoms bonded to oxygen generally get less negative as the system progresses from the initial to final state. Only for the dissociation on the (100) facet are the Pt atoms positively charged for both the transition and final states. In all cases, the Ti atoms remain positive, generally gaining greater positive charge than Ti atoms in the bare $Pt_{60}Ti_{19}$ nanoparticle. This is consistent with electron donation from Ti to Pt which in turn donates to O, following the increase in electronegativity. The situation here differs from that on $Pt_{32}Ti_6$ cluster, where the charge on the Ti atoms does not change appreciably when an O_2 molecule is adsorbed. This is likely due to the greater Ti : Pt ratio when comparing the 79 to the 38 atom clusters. The greater ratio of Ti : Pt in the $Pt_{60}Ti_{19}$ clusters results in similarly negative charges on the Pt atoms, but smaller positive charges on the Ti atoms. This will mean that more charge can be drawn from the Ti core as the system progresses to the FS, which would not be possible for the $Pt_{32}Ti_6$ clusters.

3.3.5 Conclusions. For most of the investigated features of the larger 79 atom clusters, it is possible to see similar trends to the 38 atom clusters. This implies that the present trends can be generalised also to somewhat larger nanoparticles, approaching the size of particles present in common experimental catalytic studies. For the pure Pt_{79} clusters, essentially barrier-free dissociation barriers are observed on the (111) facet for sites 10 and 11. This coincides with significant distortions of the (111) facet. However, for site 9, less distortion of the (111) facet is observed and a small dissociation barrier of 0.21 eV is found. This difference is attributed to stabilisation effects of the neighbouring (100) facet. As with the 38 atom cluster, a similar dissociation barrier of 0.34 eV is found at site 8, for the Pt_{79} and site 5 for the Pt_{38} models, on the less distorted (100) facet. Once again, dissociation barriers are observed for all sites on the $Pt_{60}Ti_{19}$ cluster, which are attributed to a notably more structurally rigid outer Pt shell when the Ti core is present.

Table 9 Pt–X^{centre} values relative to the bare clusters. Positive values show atoms being drawn out of the plane, leading to elongation of the cluster in the *y*-direction, whilst negative values show compression of the cluster in the *y*-direction. All values are given in Å

	IS		TS		FS	
	Top	Bottom	Top	Bottom	Top	Bottom
Pt_{79}-9	0.06	−0.07	0.15	−0.11	1.07	−0.12
$Pt_{60}Ti_{19}$-9	−0.06	0.01	−0.02	0.01	−0.07	−0.01
Pt_{79}-10	0.86	0.05	0.86	0.04	0.78	−0.11
$Pt_{60}Ti_{19}$-10	−0.11	0.00	−0.06	0.00	−0.11	−0.01
Pt_{79}-11	0.26	−0.13	0.24	−0.19	0.75	−0.10
$Pt_{60}Ti_{19}$-11	−0.08	0.00	0.09	−0.02	−0.11	−0.01

3.4 Nanoparticles *vs.* slab models

We found that the three-fold *fcc* site on the Pt(111) slab has similar binding energies to the central three-fold *fcc* site (position 12) on the Pt_{79} cluster, −0.86 and −0.88 eV, respectively, though, as mentioned previously, position 12 on Pt_{79} is not favourable for O_2 dissociation. It is therefore suggested that the central three-fold *fcc* site on Pt_{79} is unlikely to facilitate oxygen dissociation, due to more favourable edge hollow and bridge sites. These sites are absent on the slab Pt(111) model (as no steps or defects are included in the model) it is therefore more likely that dissociation will occur at these three-fold *fcc* hollow sites, however with a notable barrier of 0.45 eV. The rigidity of the bulk slab leads to generally weaker Pt–O bonding compared to the majority of sites on the Pt clusters. However, Pt–O bonding is found to be generally stronger than on the clusters where alloying leads to changes in electronic effects that results

Table 10 Average charges (|e|) of the initial, transition and final states of O_2 dissociation on the 79 atom clusters

	Pt charges[a]			Ti charges[b]			O charges		
	IS	TS	FS	IS	TS	FS	IS	TS	FS
Pt_{79}-8	0.28	0.25	0.44	—	—	—	−0.33	−0.38	−0.74
$Pt_{60}Ti_{19}$-8	−0.03	0.19	0.11	1.87	1.86	1.83	−0.33	−0.59	−0.74
Pt_{79}-9	0.20	0.29	0.32	—	—	—	−0.36	−0.51	−0.83
$Pt_{60}Ti_{19}$-9	−0.28	−0.16	−0.16	1.59	1.62	1.47	−0.37	−0.58	−0.74
Pt_{79}-10	0.27	0.30	0.33	—	—	—	−0.37	−0.46	−0.78
$Pt_{60}Ti_{19}$-10	−0.26	−0.12	−0.14	1.38	1.50	1.49	−0.36	−0.60	−0.78
Pt_{79}-11	0.24	0.24	0.41	—	—	—	−0.37	−0.40	−0.79
$Pt_{60}Ti_{19}$-11	−0.39	−0.22	−0.15	1.25	1.35	1.47	−0.34	−0.50	−0.78

[a] Pt atoms interacting directly with O atoms. [b] Ti atoms interacting directly with O bound Pt atoms.

in the weaker boding, as discussed earlier. Hence, the dissociation barrier on the slab model is found to lie in between the Pt clusters, with low dissociation barriers coupled with stronger Pt–O bonding, and the Ti@Pt clusters with higher dissociation barriers and weaker Pt–O bonding.

3.5 Surface flexibility

From the discussion in subsections 3.2.3 and 3.3.3, we suggest that surface flexibility has a profound effect on the potential of catalysts to activate O_2 dissociation. It is therefore of interest that Pt(111) surface lacks the ability to distort and therefore displays very different properties for oxygen dissociation when compared to pure Pt nanoparticles. We have further shown that surface flexibility is not intrinsic property of nanoparticles. Core–shell interactions stabilise the Pt shell of Ti@Pt clusters reducing flexibility. Calculating $\Delta E^{\neq}$/RMSD gives an idea of the dependence of the dissociation barrier on surface flexibility. Values for this ratio are presented in Table 11 for the 38 and 79 atom clusters. The relationship between the RMSD at the TS and dissociation barrier $\Delta E^{\neq}$ is plotted in Fig. S3,† while a plot of $\Delta E^{\neq}$/RMSD against E_b is presented in Fig. S4.†

Significantly lower $\Delta E^{\neq}$/RMSD values are obtained for the 3-fold hollow sites on the $Pt_{38}(111)$ facet, where barrier free dissociation occurs. Higher values are found for all positions on $Pt_{32}Ti_6$ as well as position 5 on Pt_{38}. This shows a strong relationship between the dissociation barrier and cluster distortion. For Pt_{79}, significantly lower values are obtained for the 3-fold hollow sites 10 and 11, where barrier free dissociation occurs. $\Delta E^{\neq}$/RMSD for positions 8 and 9 on Pt_{79} are higher than those for 10 and 11 on Pt_{79}, but lower than all positions on $Pt_{60}Ti_{19}$. In general, values for Pt_{79} are comparable with those for Pt_{38}, one more indication that the O_2 dissociation barrier and cluster distortion are strongly related.

The $\Delta E^{\neq}$/RMSD for the Pt(111) surface is 9.00 eV Å^{-1}. This is greater than for all positions on Pt_{38} or $Pt_{32}Ti_6$. The $\Delta E^{\neq}$/RMSD values for the Pt(111) slab are greater than those for Pt_{79}. This once again demonstrates the very important differences between the Pt clusters and slab. For the $Pt_{60}Ti_{19}$ cluster, the majority of the $\Delta E^{\neq}$/RMSD values are greater than those for the slab (excluding position 11), due to the reduced oxygen adsorption energy, coupled with the lack of flexibility of the Pt shell.

Table 11 Dissociation barrier $\Delta E^{\neq}$ against RMSD (eV Å^{-1}) for the 38 and 79 atom clusters at the TS. The value for the Pt(111) slab has also been calculated for comparisons[a]

38 Atom Cluster		79 Atom Cluster	
Site	$\Delta E^{\neq}$/RMSD	Site	$\Delta E^{\neq}$/RMSD
Pt_{38}-5	4.00	Pt_{79}-8	3.40
$Pt_{32}Ti_6$-5	6.20	$Pt_{60}Ti_{19}$-8	13.20
Pt_{38}-6	0.21	Pt_{79}-9	2.63
$Pt_{32}Ti_6$-6	3.09	$Pt_{60}Ti_{19}$-9	20.00
Pt_{38}-7	0.00	Pt_{79}-10	0.00
$Pt_{32}Ti_6$-7	8.86	$Pt_{60}Ti_{19}$-10	11.50
		Pt_{79}-11	0.33
		$Pt_{60}Ti_{19}$-11	7.70

[a] $\Delta E^{\neq}$/RMSD for the Pt(111) surface is 9.00 eV Å^{-1}.

4 Conclusions

We found that when the adsorption strength of the O_2 molecule on the cluster surface increases, the dissociation barrier will subsequently decrease. Hence, dissociation barriers on the alloyed Ti@Pt clusters would be found to be greater than those for the pure Pt clusters that exhibit larger E_b values. Further trends, outlined below, were discovered.

Pure Pt clusters are easily distorted when O_2 is adsorbed on the (111) facet. Furthermore, sites which are relatively easily distorted facilitate barrier-free dissociation of O_2, a trend which is not only seen for the small 38 atom clusters but also the larger 79 atom clusters. As for the alloyed Ti@Pt clusters, in all cases significant barriers are observed for all sites, which are greater than the barriers found for the pure Pt clusters.

The presence of the O_2 dissociation barriers for the Ti@Pt clusters is attributed to rigidity enhancement of the Pt shell by the Ti core. Significant electron donation is observed from Ti to Pt suggesting strong interactions between the two, which coincides with significantly less distortion of the Ti@Pt clusters, upon binding O_2, when compared to the pure Pt clusters.

The presence of the barrierless dissociation on the (111) facet of the pure Pt cluster suggest that small Pt clusters would efficiently activate O_2. However, the relatively strong adsorption strength of oxygen to the Pt surface, compared to the alloyed Ti@Pt cluster found in previous studies, means that it would be difficult to remove the resulting oxygen species from the pure Pt cluster surface. Therefore, whilst O_2 dissociation would require greater energetic input on the surface of the Ti@Pt clusters, the resulting species (following further transformations to *e.g.* H_2O or H_2O_2) would be easier to remove from the surface due to the weaker Pt–O interactions compared to the pure Pt cluster.

A very attractive development in the direction of optimal catalyst properties, resulting from findings of the present study, would be substitution of Ti in the core of Pt-based bimetallic particles by another metal (M). The ideal M core would weaken adsorption of atomic oxygen compared to pure Pt, to allow for fast ORR kinetics in the later stages of the reaction (as Ti does), but form weaker Pt–M bonds than Pt–Ti, thus maintaining the kinetic flexibility of the Pt shell which is advantageous for O_2 dissociation.

Acknowledgements

This research was funded through the RCUK doctoral training centre in hydrogen, Fuel cells and their applications (EP/G037116/1). Financial support was also provided by the EU (FP7-NMP.2012.1.1-1 project ChipCAT, Ref. No 310191) and the Spanish MICINN (CTQ2012-34969, FIS2008-02238). The authors thank COST Action MP0903: "Nanoalloys as Advanced Materials: From Structure to Properties and Applications", as well as COST Action CM1104. Much of the work has been performed under the HPC-EUROPA2 project (project number: 228398) with

the support of the European Commission – Capacities Area – Research Infrastructures. The computations described in this paper were performed in part using The University of Birmingham's BlueBEAR HPC service, which was purchased through HEFCE SRIF-3 funds, and *via* our membership of the UK's HPC Materials Chemistry Consortium, which is funded by EPSRC (EP/F067496). This work made use of the facilities of HECToR, the UK's national high-performance computing service, which is provided by UoE HPCx Ltd at the University of Edinburgh, Cray Inc and NAG Ltd, and funded by the Office of Science and Technology through EPSRC's High End Computing Programme. Computational time granted by the Barcelona Supercomputing Centre on the Marenostrum supercomputers is also gratefully acknowledged. H. A. A. thanks the Ministerio de Educación for a post-doctoral grant (SB2010-0172), Bulgarian Science Fund (grant DCVP 02/1) and FP7 project BeyondEverest for support.

References

1 Q. Fu, J. Yang and Y. Luo, *J. Phys. Chem. C*, 2011, **115**, 6864–6869.
2 M. Stamatakis and D. G. Vlachos, *ACS Catal.*, 2012, **2**, 2648–2663.
3 D. J. Schmidt, W. Chen, C. Wolverton and W. F. Schneider, *J. Chem. Theory Comput.*, 2012, **8**, 264–273.
4 J. M. Bray and W. F. Schneider, *Langmuir*, 2011, **27**, 8177–8186.
5 A. Smeltz, R. Getman, W. Schneider and F. Ribeiro, *Catal. Today*, 2008, **136**, 84–92.
6 R. Getman, W. Schneider, A. Smeltz, W. Delgass and F. Ribeiro, *Phys. Rev. Lett.*, 2009, **102**, 076101.
7 W. Chen, D. Schmidt, W. F. Schneider and C. Wolverton, *J. Phys. Chem. C*, 2011, **115**, 17915–17924.
8 R. B. Getman, Y. Xu and W. F. Schneider, *J. Phys. Chem. C*, 2008, **112**, 9559–9572.
9 D.-H. Lim and J. Wilcox, *J. Phys. Chem. C*, 2011, **115**, 22742–22747.
10 M. Kettner, W. B. Schneider and A. A. Auer, *J. Phys. Chem. C*, 2012, **116**, 15432–15438.
11 Y. Xu, W. A. Shelton and W. F. Schneider, *J. Phys. Chem. A*, 2006, **110**, 5839–5846.
12 D. Cheng and W. Wang, *Nanoscale*, 2012, **4**, 2408–2415.
13 A. Chandan, M. Hattenberger, A. El-kharouf, S. Du, A. Dhir, V. Self, B. G. Pollet, A. Ingram and W. Bujalski, *J. Power Sources*, 2013, **231**, 264–278.
14 A. Pollet, J. E. Newton, J. A. Preece and O. J. Curnick, *ECS Trans.*, 2011, 2165–2173.
15 O. J. Curnick, P. Mendes and B. Pollet, *ECS Trans.*, 2010, 557–561.
16 O. J. Curnick, P. M. Mendes and B. G. Pollet, *Electrochem. Commun.*, 2010, **12**, 1017–1020.
17 B. Li and S. H. Chan, *Int. J. Hydrogen Energy*, 2013, **38**, 3338–3345.
18 P. Mani, R. Srivastava and P. Strasser, *J. Power Sources*, 2011, **196**, 666–673.
19 R. Othman, A. L. Dicks and Z. Zhu, *Int. J. Hydrogen Energy*, 2012, **37**, 357–372.
20 J.-Y. Choi, R. S. Hsu and Z. Chen, *J. Phys. Chem. C*, 2010, **114**, 8048–8053.
21 L. Calvillo, M. Gangeri, S. Perathoner, G. Centi, R. Moliner and M. Lázaro, *Int. J. Hydrogen Energy*, 2011, **36**, 9805–9814.
22 B. Seger and P. V. Kamat, *J. Phys. Chem. C*, 2009, **113**, 7990–7995.
23 P. C. Jennings, B. G. Pollet and R. L. Johnston, *Phys. Chem. Chem. Phys.*, 2012, **14**, 3134–3139.
24 P. C. Jennings, B. G. Pollet and R. L. Johnston, *J. Phys. Chem. C*, 2012, **116**, 15241–15250.
25 G. Kresse and J. Hafner, *Phys. Rev. B: Condens. Matter Mater. Phys.*, 1993, **47**, 558–561.
26 G. Kresse, *Phys. Rev. B: Condens. Matter Mater. Phys.*, 1996, **54**, 11169–11186.
27 G. Kresse and J. Furthmüller, *Comput. Mater. Sci.*, 1996, **6**, 15–50.
28 G. Kresse and J. Hafner, *Phys. Rev. B: Condens. Matter Mater. Phys.*, 1994, **49**, 14251–14269.
29 P. E. Blöchl, *Phys. Rev. B: Condens. Matter Mater. Phys.*, 1994, **50**, 17953–17979.
30 G. Kresse, *Phys. Rev. B: Condens. Matter Mater. Phys.*, 1999, **59**, 1758–1775.
31 J. P. Perdew, K. A. Jackson, M. R. Pederson, D. J. Singh and C. Fiolhais, *Phys. Rev. B: Condens. Matter Mater. Phys.*, 1992, **46**, 6671–6687.
32 J. Perdew, J. Chevary, S. Vosko, K. Jackson, M. Pederson, D. Singh and C. Fiolhais, *Phys. Rev. B: Condens. Matter Mater. Phys.*, 1993, **48**, 4978.
33 D. Sheppard, P. Xiao, W. Chemelewski, D. D. Johnson and G. Henkelman, *J. Chem. Phys.*, 2012, **136**, 074103.
34 J. Kästner and P. Sherwood, *J. Chem. Phys.*, 2008, **128**, 014106.
35 R. F. W. Bader, *Atoms in Molecules: a Quantum Theory*, Oxford University Press, New York, 1994.
36 W. Tang, E. Sanville and G. Henkelman, *J. Phys.: Condens. Matter*, 2009, **21**, 084204.
37 S. M. Kozlov and K. M. Neyman, *Top. Catal.*, 2013, **56**, 867–873.
38 H. Steininger, S. Lehwald and H. Ibach, *Surf. Sci.*, 1982, **123**, 1–17.
39 C. Puglia, A. Nilsson, B. Hernnäs, O. Karis, P. Bennich and N. Mårtensson, *Surf. Sci.*, 1995, **342**, 119–133.
40 A. Eichler and J. Hafner, *Phys. Rev. Lett.*, 1997, **79**, 4481–4484.
41 K. Gustafsson and S. Andersson, *J. Chem. Phys.*, 2004, **120**, 7750–7754.
42 Z. Duan and G. Wang, *Phys. Chem. Chem. Phys.*, 2011, **13**, 20178.
43 D. J. Miller, H. Öberg, L.-A. Näslund, T. Anniyev, H. Ogasawara, L. G. M. Pettersson and A. Nilsson, *J. Chem. Phys.*, 2010, **133**, 224701.
44 L. Qi, J. Yu and J. Li, *J. Chem. Phys.*, 2006, **125**, 054701.
45 V. Šljivančanin and B. Hammer, *Surf. Sci.*, 2002, **515**, 235–244.

46 B. Stipe, M. Rezaei, W. Ho, S. Gao, M. Persson and B. Lundqvist, *Phys. Rev. Lett.*, 1997, **78**, 4410–4413.
47 J. R. Kitchin, J. K. Nørskov, M. A. Barteau and J. G. Chen, *J. Chem. Phys.*, 2004, **120**, 10240–10246.
48 P. Gambardella, V. Šljivančanin, B. Hammer, M. Blanc, K. Kuhnke and K. Kern, *Phys. Rev. Lett.*, 2001, **87**, 056103.
49 P. Feibelman, S. Esch and T. Michely, *Phys. Rev. Lett.*, 1996, **77**, 2257–2260.
50 M. Shao, A. Peles and K. Shoemaker, *Nano Lett.*, 2011, **11**, 3714–3719.
51 Z. Duan and G. Wang, *J. Phys. Chem. C*, 2013, **117**, 6284–6292.